

Article

Alkali Treatment of Anodized Titanium Alloys Affects Cytocompatibility

Alicja Kazek-Kęsik ^{1,*}, Katarzyna Leśniak ¹, Beata Urszula Orzechowska ², Marek Drab ³,
Agnieszka Wiśniewska ² and Wojciech Simka ^{1,*}

¹ Faculty of Chemistry, Silesian University of Technology, B. Krzywoustego Street 6, 44-100 Gliwice, Poland; katarzyna.lesniak94@gmail.com

² Laboratory of Virology, Institute of Immunology and Experimental Therapy (IIET), Polish Academy of Sciences, Rudolfa Weigla Street 12, 53-114 Wrocław, Poland; orzechow@iitd.pan.wroc.pl (B.U.O.); drobna@iitd.pan.wroc.pl (A.W.)

³ USI, Unit of Nanostructural Biointeractions, Laboratory of Virology, Institute of Immunology and Experimental Therapy (IIET), Polish Academy of Sciences, Rudolfa Weigla Street 12, 53-114 Wrocław, Poland; mdmd007@wp.pl

* Correspondence: alicja.kazek.kesik@polsl.pl (A.K.-K.); wojciech.simka@polsl.pl (W.S.); Tel.: +4832-237-1754 (A.K.-K.); +4832-237-2605 (W.S.)

Received: 31 October 2017; Accepted: 28 December 2017; Published: 3 January 2018

Abstract: In this paper, the surface modification of titanium alloys Ti-15Mo, Ti-13Nb-13Zr, and Ti-6Al-7Nb is presented as a material for dental implants. The conditions of the plasma electrolytic oxidation process and alkali treatment were designed in this way to enhance the biological properties of the surface of promising Ti alloys. The differences in their surface morphology and, consequently, in their biological properties were discussed. The bioactivity of the samples was examined in vitro using simulated body fluid, and Saos-2 osteoblast cells. On all the samples, characteristic apatite particles were formed. However, compared to as-ground, natively-oxidized bare alloys, the plasma electrolytic oxidation (PEO)-modified surface of the Ti-13Nb-13Zr alloy showed the highest cytocompatibility for Saos-2 osteoblast cells, and a beneficial gain of cytocompatibility was also achieved in the treated sample of Ti-6Al-7Nb. In contrast, the modification of the Ti-15Mo alloy did not influence the adhesion and proliferation of osteoblast cells.

Keywords: titanium alloys; anodization; alkali treatment; cytocompatibility

1. Introduction

Long-term implants should exhibit cytocompatibility and bioactivity for potential application in bone tissue engineering. Bone implants are usually made of titanium. Their surface should favor cell adhesion and allow for ion exchange, which is necessary for tissue integration. The penetration of cell fluids into the titanium surface, and not disturbing the bone remodeling process, is also crucial [1].

For Ti-based materials, different techniques are used for their surface treatment; e.g., ion implantation, physical or chemical vapor deposition, electrophoresis, or anodization were the selected compounds formed on the metal surface. A plasma electrolytic oxidation (PEO) process is a kind of anodization process for the formation of a very good adhesive and porous layer [2]. The solution for Ti-based materials might be designing a surface with a desirable microstructure and chemical composition [3–5]. Selected compounds might be incorporated into the porous oxide layer formed on the substrate. This method of surface treatment might be cost-effective (the cost depends on the price of chemical reagents and mainly on the price of substrate), not time-consuming, and easily reproducible [6,7]. Surface treatment of these materials by the PEO process enhances the osseointegration process and creates antibacterial properties, due to the incorporation of desirable

compounds into the layer [8,9]. In medical applications, titanium alloys might be used, such as Ti-xMo and Ti-xNb-xZr. Selected β -phase and $\alpha + \beta$ phase Ti alloy presents mechanical properties close to the selected natural bone (e.g., Ti-15Mo alloy or Ti-13Nb-13Zr) [10,11]. The mentioned titanium alloys are composed only of biocompatible elements and, thus, products of their corrosion are not a health problem for humans [12]. Implants made by titanium or Ti-6Al-4V alloy are currently available at the market; however, producers are still looking for new materials that will present multifunctional properties (mechanical and biological). On the other hand, many papers present coatings to protect surface of Ti-6Al-4V against corrosion in human body fluid. Coatings might exhibit high adhesion to the substrate, but during implantation process into bone, the protective layer might be destroyed. Accumulation of the ions released from the Ti-6Al-4V alloy are accumulated in tissue around implanted material [13]. Aluminum plays a role in encephalopathy, osteomalacia, and anemia. It was reported that aluminum phosphate compounds induce cytotoxic effects for the HT-29 cell line at very low concentration (25 $\mu\text{g}/\text{mL}$) [14]. Zaffe et al. [15] reported that aluminum evolved from a Ti-6Al-4V implant caused local inflammation in parts of lamellar bone. In addition to selected ions, which might be released from materials, it was proven that TiO_2 nanoparticles are accumulated in the cortex and hippocampus of the brain causing problems in the central nervous system [16]. Particles of TiO_2 with dimensions less than 100 nm may induce apoptosis and inflammation and change the gene expression of selected cells. Thus, investigations on whether the material will be corrosion-resistant, or if corrosion products will be inert for living tissue, are desirable.

Formation of porous titanium oxide coatings is beneficial for bone tissue integration. However, new coatings, including multilayer ceramic coatings, are still being sought to improve cell adhesion and new bone formation. It was reported that small amounts of wollastonite (CaSiO_3) enhances osteoblast cell proliferation [17]. Addition of Si also induced apatite formation [18]. Proliferation and alkaline phosphatase activity (ALP) was improved when the TiO_2 porous layer was doped by Si ions using plasma immersion ion implantation [19]. Hu et al. [20] reported that deposition of calcium silicate on the TiO_2 layer by electron beam evaporation increased osteoblast cell MG-63 viability up to seven days. It was also found that the nanostructure of biomimetic material formed on macroscale coatings improves bone cell functions and osteogenic capacity. The mesoporous structure of coatings also increased bone anchorage with the implant [21]. A dual microstructure (macro and nano) was formed using a two-step technique, e.g., plasma electrolytic oxidation and hydrothermal treatment or alkali treatment. The characteristic nano-flake structure was formed on the Ti plates due to only immersion of the substrate in sodium hydroxide and then hydrothermally treated in CaHPO_4 solution. It should be mentioned that the effect of surface treatment strongly depended on the substrate (chemical composition of Ti alloy) and the methods of surface pretreatment [22]. A favorable nanostructure might also be prepared using anodization and dip coating. Biological investigations showed higher interaction of cells with macro- and mesoporous surfaces compared to smooth surfaces [23]. Additional surface treatment did not decrease the attachment of the oxide layer to the substrate, which is important for the quality of implant.

Mesoporous structure promotes bone cells attachment, while macropores promote the osseointegration process [24]. The synergistic effect between micro and nano-topography surfaces was evaluated using canine bone marrow mesenchymal stem cells (BMSCs) [25]. Bone cell adhesion and proliferation were promoted by functional groups, which allowed for adsorption of proteins and bone cells. A post-grafting technique might improve cell differentiation, for example, due to the presence on surface $-\text{NH}_2$ groups. In addition to topography and chemical composition, a large number of other parameters induce or limit cytocompatibility of the surface; thus, the materials are still evaluated experimentally.

To obtain the multifunctional properties of Ti alloys, their surface may also be enriched using selected drugs used in dentistry, like doxycycline, clindamycin, vancomycin, or gentamycin, which might be loaded into the biomaterial. However, the formation of the layer with the biologically-active substance needs additional techniques for coating formation and control of drug

release. In this paper, we proposed another additional surface treatment—an alkali treatment. Immersion of the PEO layer in 1 M of NaOH caused slight changes in the surface morphology, which was favorable for bone cell adhesion. The methods might also be applied to modify the surface of three promising vanadium-free titanium alloys, Ti-15Mo, Ti-13Nb-13Zr, and Ti-6Al-7Nb. The evaluation of bioactivity, cytocompatibility of these layers was conducted.

2. Experimental

2.1. Formation of Coatings

Titanium alloys Ti-15Mo, Ti-13Nb-13Zr, and Ti-6Al-7Nb (BIMO Metals, Wroclaw, Poland) were anodized and alkali-treated according to the procedure, which is presented in detail in [26]. The condition to obtain the most favorable microstructure and chemical composition for materials, which may find application for dental implants, was determined. An anodizing bath was composed of calcium hypophosphite and wollastonite powder. After anodization, all the anodized Ti samples were immersed in a 1 M of NaOH solution at 60 °C for 8 h.

2.2. Bioactivity and Cytocompatibility

2.2.1. Simulated Body Fluid

Bioactivity investigations were performed in a protein-free simulated body fluid (SBF) with an ion concentration simulating that of human blood plasma [27]. The SBF solution contained the following ions at the respective concentrations ($\text{mM}\cdot\text{dm}^{-3}$): Na^+ 142, K^+ 5, Mg^{2+} 1.5, Ca^{2+} 2.5, Cl^- 147.8, HCO_3^{3-} 4.2, HPO_4^{2-} 1.0, and SO_4^{2-} 0.5. The SBF was prepared by dissolving reagent-grade NaCl, NaHCO_3 , KCl, $\text{K}_2\text{PO}_4\cdot 3\text{H}_2\text{O}$, $\text{MgCl}_2\cdot 6\text{H}_2\text{O}$, CaCl_2 , and Na_2SO_4 in distilled water, which was adjusted to a pH of 7.40 using tris(hydroxymethyl) aminomethane and 1 M of HCl at 36.5 °C. After the PEO process, the specimens were immersed in the SBF for a total of four weeks. After each week, the formation of apatites was analyzed by observations using a scanning electron microscope (SEM, Hitachi TM-3000, Tokyo, Japan; accelerating voltage = 15 kV). Before SEM observation, the samples were covered by a thin gold layer (Cressington Sputter Coater 108 Auto, Cressington Scientific Instruments UK, Watford, UK).

2.2.2. Cytocompatibility

Cell Culture

Human osteosarcoma cell line Saos-2 (ATCC[®] HTB-8, Rockville, MD, USA) was cultured in McCoy's 5A medium (Biowest, Nuaille, France) supplemented with 10% (*v/v*) heat-inactivated fetal calf serum (FCS), 1% penicillin/streptomycin at 37 °C in 5% CO_2 , in a 95% air atmosphere with 100% humidity. The culture medium was changed every three days. The cells were passaged by lifting with trypsin/ethylenediaminetetraacetic acid (EDTA) and cultivated until they reached 80% confluence. They were then centrifuged and resuspended in complete medium before they were plated on the samples.

Initial Cell Adhesion and Cell Morphology

The samples were washed three times with 70% ethanol and complete McCoy's culture medium. The washed samples were placed in 24-well tissue culture plates (Falcon, Becton Dickenson and Company, Franklin Lakes, NJ, USA), and then 5×10^4 cells per sample (in 1 cm^3 complete McCoy's medium) were added and incubated for 24 h. Cells were maintained at 37 °C in a humidified incubator in an atmosphere of 5% CO_2 . Cells were washed twice with cold phosphate-buffered saline (PBS) in order to remove the non-adherent cells and then fixed with paraformaldehyde. Subsequently, the cells were permeabilized with 0.1% Triton X-100 and rinsed three times with PBS. The nonspecific binding sites were blocked in 1% (*w/v*) bovine serum albumin (BSA) in PBS with 0.1% Triton X-100 (PBST).

To observe the cell adhesion and the overall morphology of the adhering cells, the actin filaments of the cells were stained with rhodamine-conjugated phalloidin (Invitrogen Molecular Probes, Carlsbad, CA, USA). To label the nuclei, the cells were pretreated with a fluorescent dye that binds to the DNA by intercalation, Hoechst No. 33342 (Invitrogen, Carlsbad, CA, USA), at a concentration of $0.3 \mu\text{g}\cdot\text{cm}^{-3}$. The morphology of the cells was examined by confocal laser scanning microscopy (Zeiss Cell Observer SD Spinning Disk Yokogawa CSU-X1A 5000; lasers: 405, 488, 561, and 635 nm; and an EMCCD iXon3 885 camera, Andor Technology, Belfast, Northern Ireland, UK).

Statistical Analysis

Each sample was visualized under a $100\times$ oil immersion lens, and six fields of view were randomly chosen for analysis. Experimentation was carried out for three independent samples. The images were processed, and the cell counts were obtained using ImageJ (NIH, Bethesda, MD, USA). ANOVA tables with a multiple-comparison Fisher's test were determined to assess significant differences between the field of view (FOV) (* $p < 0.05$).

Scanning Electron Microscopy at a Low Voltage (LV-SEM)

Scanning electron microscopy of the cells cultured on modified alloys was processed at a low accelerating voltage of the primary beam without any coating of the samples.

The samples were rinsed with PBS at room temperature and fixed with 2.5% glutaraldehyde in 0.1 M of cacodylate buffer for 30 min at room temperature. The samples were washed five times for 10 min in 0.1 M of cacodylate buffer at room temperature and redirected to dehydration in a series of ethanol solutions in steps at 25%, 40%, 60%, 80%, 99.8%, and 99.8%, each lasting 1 h at 4 °C.

All the samples designed for imaging at room temperature underwent critical point drying with 99.8% ethanol exchanged for liquid CO₂ in an automatized manner (CPD300 AUTO, Leica Microsystems, Vienna, Austria) and were imaged with a cross-beam scanning electron microscope equipped with a Schottky field-emission cathode (Auriga 60, Carl Zeiss, Oberkochen, Germany) at a 1.2 kV accelerating voltage. A dual-imaging mode was applied with simultaneous recording of the secondary electrons SE2 (Everhart-Thornley detector), SE1 (In-Lens detector), and back-scattered electrons energy-filtered with a low cut-off electrostatic grid filter (energy-selective BSE detector, EsB). The EsB detector ensured the electron yield as a function of the retarding (negative) cut-off potential of the detector grid. The retarding potential was set to a level of 100 eV energy lower than the energy of the primary beam (1100 eV retarding potential filter when a primary beam of 1200 keV was used) depending on the sample. For all the imaged samples, the material contrast was achieved with an EsB detector by recording the back-scattered electrons with low energy losses (low-loss BSE, LL-BSE) in real-time and simultaneously with other detectors. The material contrast (EsB with retarding grid potential) could be reliably correlated with topographic features (ET and In-lens detectors) on the samples and served as the major source of information regarding the biological objects on the studied substrate.

The images represent electron EsB energy-filtered maps and are correlated with the Everhart-Thornley or in-lens detection directly from the sample surfaces and without coating or any additional contrast applied to approach the native composition of the bio-sample and original substrate composition as closely as possible.

3. Results and Discussion

The conditions for the surface treatment were chosen based on our previous investigation and the results presented in [26]. The microstructure of the coatings of the Ti alloys was different due to the chemical composition of the Ti alloy, which influences the oxide layer formation. Thus, the results of the alkali treatment were also variable. To improve the biocompatibility of the oxide layers, the post-treatment using an alkali solution was provided. Two different solutions, such as NaOH and KOH, was used for the formation of nano-flake structures of biomimetic compounds on the top of the porous oxide layer. The concentration of these solutions and the temperature of the sample incubation

influence the formation characteristics of the flakes on the top of the oxide layer. Finally, we confirmed that immersion of anodized Ti alloy samples in a solution containing 1 M NaOH of 60 °C for 8 h was the most favorable for anodized surfaces. Titanium alloy samples after anodization and the alkali treatment process were labeled as follows: TM-AT, TNZ-AT, and TAN-AT for Ti-15Mo, Ti-13Nb-13Zr, and Ti-6Al-7Nb alloys, respectively.

Figure 1 presents the representative SEM images of the treated Ti alloy surfaces.

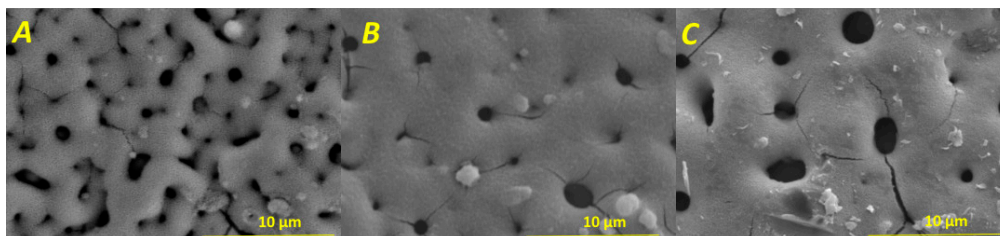


Figure 1. Morphology of the anodized and alkali-treated Ti-15Mo (A); Ti-13Nb-13Zr (B); and Ti-6Al-7Nb alloy (C).

All the coatings were porous, however, the morphology of the treated Ti-15Mo alloy was slightly different compared with coated Ti-13Nb-13Zr and Ti-6Al-7Nb alloy surfaces. The chemical composition of the layers was also determined by the kind of treated Ti surface. All the coatings were mainly composed of Ca, P, and Ti compounds as determined by X-ray photoelectron spectroscopy (XPS) spectroscopy [26]. It was confirmed that on all of the surfaces, the titanate-based compounds were formed. However, the Na 1s line could not be precisely defined on the XPS spectra, and it was not clear that Na–O or Na–OH was formed on treated surfaces. For all of the coatings the Si atom was detected, and its line corresponds to the structure of wollastonite (CaSiO₃) particles, incorporated into oxide layers from the anodizing bath. The Ca–O bond was detected for all coatings, which also corresponds to CaSiO₃. The highest concentration of calcium and oxygen atoms was determined for the TAN-AT sample, then for TNZ-AT surface, and the least for TM-AT.

Most of the coating was in the amorphous phase due to the presence of amorphous anatase (TiO₂) and disordered incorporated particles of wollastonite. Wollastonite particles were melted and closed in the oxide layer during the surface anodization. The coating formed on the Ti-15Mo alloy was less porous and more compact. This titanium alloy was also anodized at a lower voltage (350 V) compared with the condition for the surface treatment of the two other Ti alloys. The conditions of the surface treatment were evaluated based on our previous investigations, which are presented in [26]. The influence of type of titanium alloys on the anodization results and the further surface modification (e.g., the formation of the ceramic coating) were presented in [28]. The differences in the coating morphologies determined the formation of apatite and biological properties.

Bioactivity and Cytocompatibility of the Coatings

The titanium alloy samples were immersed in simulated body fluid at 37 °C for four weeks. Figure 2 presents the morphologies of the coatings after each week of immersion. After one week, small spherical particles were formed on the TM-AT.

The apatite particles were better distributed than those on the TAN-AT surface. Formed particles were larger and covered the large part of the PEO-layer compared with the result observed for the TM-AT surface. After two weeks, the particles grew on the TM-AT and TAN-AT samples. The surface of TAN-AT was completely covered by the apatite layer. On the TNZ-AT, small irregular particles of apatite were observed after two weeks of the sample's immersion. The particles of apatite had grown on the TM-AT and TNZ-AT surfaces during three and four weeks of immersion. The characteristic round particles of apatite covered almost all the surfaces. On the TAN-AT surface, the apatite was formed faster and generated additional apatite layers. Similar results were reported by Wei et al. [29].

The anodized and chemically-treated surface in the NaOH solution enhances the formation of apatite, and this mechanism has been addressed in several publications and serves for the assessment of the surface bioactivity [30–32]. In vivo, the apatite layer does not occur on the surface, and the osteoblast cells are mainly responsible for matrix production and tissue mineralization [33,34].

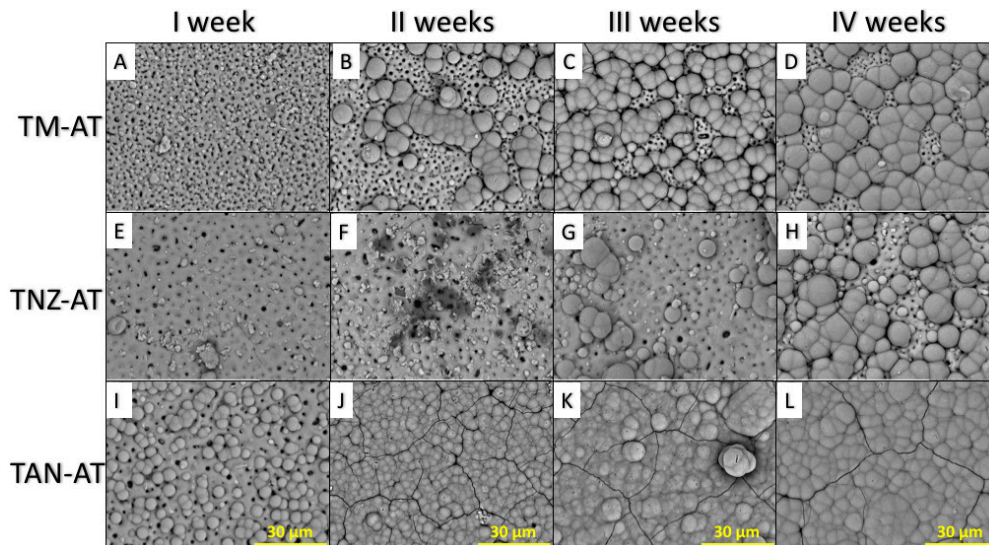


Figure 2. SEM (Scanning Electron Microscopy) images of the coated TM-AT, TNZ-AT, and TAN-AT samples after one (A,E,I), two (B,F,J), three (C,G,K) and four (D,H,L) weeks immersion in SBF (Simulated Body Fluid) solution.

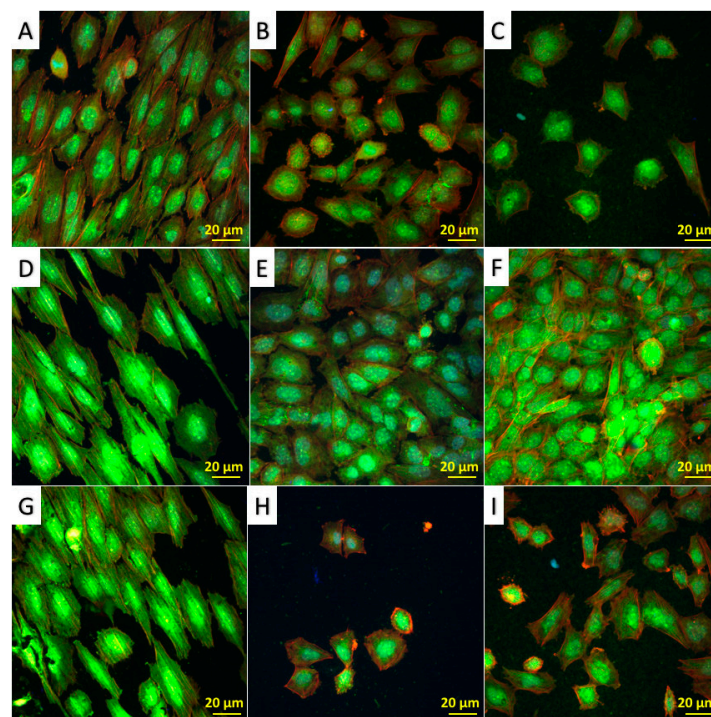


Figure 3. Fluorescence microscope images of cells after 24 h of culture on (A) TM; (B) TM-PEO; (C) TM-AT; (D) TNZ; (E) TNZ-PEO; (F) TNZ-AT; (G) TAN; (H) TAN-PEO; and (I) TAN-AT samples; bar = 20 μm . Staining occurred using rhodamine-conjugated phalloidin.

The adhesion of the osteoblast-like Saos-2 cells to the reference and modified titanium alloy samples was investigated after 24 h of culture. The cells were well adhered on all the surfaces (Figure 3).

The cells were well distributed on the surfaces with no obvious changes in their appropriate morphology. The number of cells was similar between the reference sample of the TM and TNZ and the samples after plasma electrolytic oxidation (Figure 4).

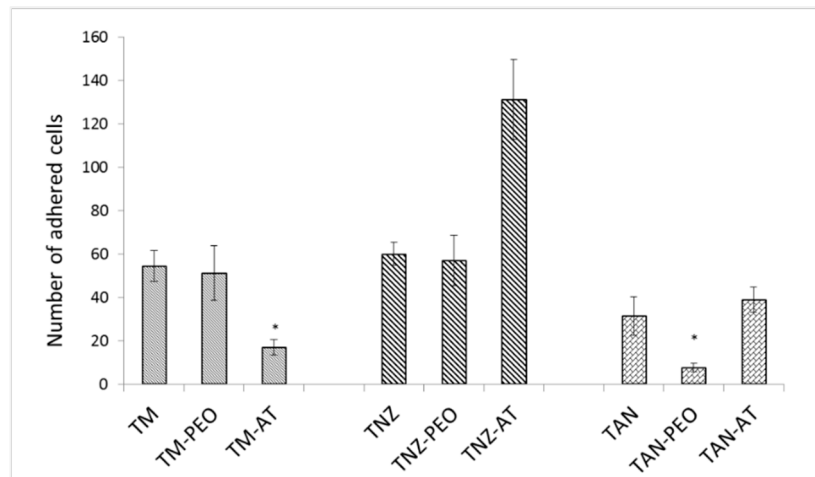


Figure 4. The cell numbers of Saos-2 cells adhered on the surface of the original TM, TAN, and TNZ and the treated titanium alloys' surface after 24 h of incubation. The bars represent the means and the error bars represent the standard deviations for $n = 6$ FOV, * $p < 0.05$.

For the TAN-PEO sample, the number of adhered cells was lower compared to the unmodified surface of titanium alloy (TAN). Alkali treatment of the anodized samples influenced the number of adhered Saos-2 cells. The highest number of cells adhered to the TNZ-AT sample. The TNZ-AT surface was completely covered by cells (Figure 3F). Immersion of the anodized TAN sample in the NaOH solution increased the number of adhered cells. The surface area of the TNZ and TNZ-PEO (Figure 3D,E) were confluent covered by adhered cells. Immersion of the TM-PEO sample in the alkali solution was not favorable for the adhesion of Saos-2 cells.

The morphologies of the osteoblast cells adhered on the surfaces of TNZ, TNZ-PEO, and TNZ-AT samples were examined using a scanning electron microscope with three detection systems which allowed for correlated identification of several complementary aspects of cell features. The topography of the cells that were imaged by SE-2 electron detection (ET-detector) showed high confluence of the cell layer on the TNZ and TNZ-PEO substrates (Figure 5A,D, respectively) with less dense coverage on TNZ-AT (Figure 5G).

On the three substrates, the cells acquired a flattened phenotype and were well spread, which demonstrated signs of favorable bio-compatibility of all three applied functionalization methods. The clear difference in the lateral polarity of the cells was observed between the non-functionalized (TNZ) and functionalized surfaces (TNZ-PEO and TNZ-AT), which were best visible with SE1 detection (In-Lens SE1 detector), as shown Figure 5B,E,H, respectively. The non-coated TNZ surface that shows the texture of the parallel grooves forced the cells to elongate their contours and their nuclei along the direction of the grooves and indirectly speak for polarized tensegrity induced in the cells by the anisotropic geometry of the TNZ substratum (panel B). In contrast, the surface coatings in TNZ-PEO (panel E) and TNZ-AT (panel H) efficiently masked the underlying alloy texture and overlaid it with their own isotropic perforated texture that directly affected the cell lateral polarization with the isotropic contours of the cells. The inter-cellular spaces were best visualized with an energy-filtered detection (EsB detector), and the EsB-generated chemical contrast between the substrata and the cells.

EsB detection helped visualize fine filopodia with which the cells established mutual multiple direct contacts (Figure 5C,F,I). A strong impact of the substratum texture's anisotropy will presumably affect the geometry of the cellular component on implants that may limit adaptive processes in the case of TNZ in future in situ applications. In contrast, the modified surfaces (TNZ-PEO and TNZ-AT) enable better responsiveness of the cells to an organism's spatial cues, such as tissue strain and stresses, which are critical for endogenous bone architecture. TNZ-PEO and TNZ-AT promise better responsiveness to the natural mechanical architecture of the organism than non-modified TNZ, and the latter strongly limits the force homeostasis of the tissue by overriding it with artificial alloy texture (Figure 5). On these samples, the highest number of the cells adhered after 24 h of incubation.

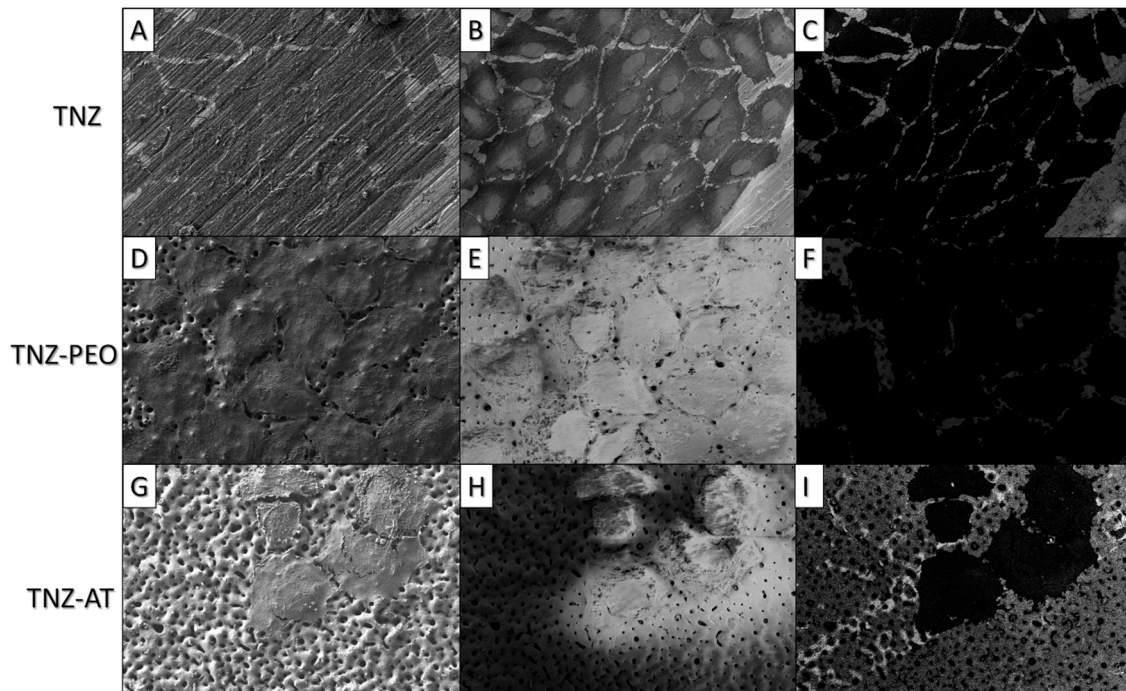


Figure 5. SEM imaging of cells cultivated on reference (TNZ) or modified alloys (TNZ-PEO, TNZ-AT). The topography of the cells, imaged by SE-2 electron detection (ET-detector) (A,D, respectively), with less dense cell coverage on TNZ-AT (G). The lateral polarity was visualized with SE1 detection (In-Lens SE1 detector) (B,E,H, respectively) with polarized tensilegrity induced in the cells by anisotropic geometry of the TNZ substratum (B), whereas the surface coatings in TNZ-PEO (E) and TNZ-AT (H) efficiently masked the underlying alloy texture with observed isotropic contours of the cells. The intercellular spaces visualized with energy-filtered detection (EsB detector) allowed visualization of the fine filopodia, which form multiple intercellular direct contacts (C,F,I). A strong impact of the substratum texture's anisotropy in the case of TNZ was prevented with modification of the surfaces (TNZ-PEO and TNZ-AT) and, thus, promised an easier response to local cues and better adaptation of the cells to an organism's bone architecture.

The surface roughness, wettability, chemical composition, and charge of the surface influence the reaction at the interface of the biomaterial/reagents and the cell adhesion. The mechanisms of bone formation can be divided into two main stages: primary and secondary osteogenesis (ossification) [35]. During the first step, the endochondral ossification occurs, which is a combination of the ground substance with fibril (10–20 nm of diameter) bundles of collagen [36]. High concentrations of various ions are delivered, and the process of mineralization starts. The mineralization is first unorganized and forms a “woven” tissue structure. Collagen type-I that is present in the ground substance is not organized into lamellae yet. The clusters of hydroxyapatite are not deposited within the collagen of the surrounding proteoglycan matrix. It was reported that collagen type-I does not appear to play a

direct role in the mineralization process during the first stage [36]. In the second phase, the primary woven bone tissue undergoes remodeling into highly organized tissue, such as parallel-fibered bone, which makes up the osteons of the Haversian canal system. The nanoscopic platelets of hydroxyapatite become oriented and aligned within the collagen fibers, and osteons become densely packed. In the second step, osteoblasts secrete collagen fibrils (with a diameter of approximately 80 nm) and collagen fibers undergo a progressive mineralization process. The surface properties of biomaterial implanted into the bone should allow for the adsorption of ions, proteins, and cells. The porous and easily wettable surface is more favorable for bone formation due to possibility of the matrix fluid penetration into the material.

4. Conclusions

Alkali treatment is a favorable method for PEO layers to change their biological properties in a fast and simple manner. The final effect of the titanium alloys' surface modification strongly depends on their chemical composition. The anodization process, and then immersion in the NaOH solution, might be designed to obtain a desirable biological response.

The treated surface of the TNZ alloy was the most cytocompatible with Saos-2 cells. Alkali treatment of the anodized TNZ surface allows the highest number of cells to adhere. The alkali treatment of the TM and TAN surfaces was not favorable for cell adhesion, but the surfaces were also not cytotoxic. On all the samples, the cells were well adhered without any change in morphology.

Acknowledgments: This work was supported by the Polish Ministry of Science and Education under research project No. IP 2012 0459 72 and by Rector's Grant in the field of research and development (Silesian University of Technology, Poland [04/010/RG]17/0049] grant.

Author Contributions: Alicja Kazek-Kęsik, Beata Urszula Orzechowska and Wojciech Simka conceived and designed the experiments; Alicja Kazek-Kęsik, Beata Urszula Orzechowska and Agnieszka Wiśniewska performed the experiments; Alicja Kazek-Kęsik, Marek Drab and Wojciech Simka analyzed the data; Katarzyna Leśniak contributed reagents/materials/analysis tools; Alicja Kazek-Kęsik wrote the paper.

Conflicts of Interest: The authors declare no conflict of interest.

References

1. Amini, A.R.; Laurecin, C.T.; Nukavarapu, S.P. Bone tissue engineering: Recent advances and challenges. *Crit. Rev. Biomed. Eng.* **2012**, *40*, 363–408. [[CrossRef](#)] [[PubMed](#)]
2. Lin, C.S.; Chen, M.T.; Liu, J.H. Structural evolution and adhesion of titanium oxide film containing phosphorus and calcium on titanium by anodic oxidation. *J. Biomed. Mater.* **2008**, *85A*, 378–387. [[CrossRef](#)] [[PubMed](#)]
3. Rokosz, K.; Hryniewicz, T.; Dudek, Ł.; Matýsek, D.; Valíček, J.; Harničárová, M. SEM and EDS analysis of surface layer formed on titanium after plasma electrolytic oxidation in phosphoric acid with the addition of copper nitrate (NanoOstrava 2015). *J. Nanosci. Nanotechnol.* **2016**, *16*, 7814–7817. [[CrossRef](#)]
4. Rokosz, K.; Hryniewicz, T.; Raaen, S.; Chapon, P. Investigation of porous coatings obtained on Ti-Nb-Zr-Sn alloy biomaterial by plasma electrolytic oxidation: Characterisation and modelling. *Int. J. Adv. Manuf. Technol.* **2016**, *87*, 3497–3512. [[CrossRef](#)]
5. Rokosz, K.; Hryniewicz, T.; Dalibor, M.; Raaen, S.; Valicek, J.; Dudek, Ł.; Harnicarova, M. SEM, EDS and XPS analysis of the coatings obtained on titanium after plasma electrolytic oxidation in electrolytes containing copper nitrate. *Materials* **2016**, *9*, 318. [[CrossRef](#)] [[PubMed](#)]
6. Rokosz, K.; Hryniewicz, T.; Raaen, S.; Chapon, P.; Dudek, Ł. GDOES, XPS and SEM with EDS analysis of porous coatings obtained on titanium after plasma electrolytic oxidation, surface and interface analysis. *Adv. Mater. Sci.* **2016**, *49*, 303–315.
7. Rokosz, K.; Hryniewicz, T.; Malorny, W. Characterisation of porous coatings obtained on materials by plasma electrolytic oxidation. *Mater. Sci. Forum* **2016**, *862*, 86–95. [[CrossRef](#)]
8. Lu, X.; Mohedano, M.; Blawert, C.; Matykina, E.; Arrabal, R.; Kainer, K.U.; Zheludkevich, M.L. Plasma electrolytic oxidation coatings with particle additions—A review. *Surf. Coat. Technol.* **2016**, *307*, 1165–1182. [[CrossRef](#)]

9. Shin, K.R.; Kim, J.S.; Kim, G.W.; Yang, H.W.; Ko, J.G.; Shin, D.H. Effects of concentration of Ag nanoparticles on surface structure and in vitro biological responses of oxide layer on pure titanium via plasma electrolytic oxidation. *Appl. Surf. Sci.* **2015**, *347*, 574–582. [[CrossRef](#)]
10. Oliveira, N.T.C.; Guastaldi, A.C. Electrochemical stability and corrosion resistance of Ti-Mo alloys for biomedical applications. *Acta Biomater.* **2009**, *5*, 399–405. [[CrossRef](#)] [[PubMed](#)]
11. Wang, X.; Li, Y.; Xiong, J.; Hodgson, P.D.; Wen, C. Porous TiNbZr alloy scaffolds for biomedical applications. *Acta Biomater.* **2009**, *5*, 3616–3624. [[CrossRef](#)] [[PubMed](#)]
12. Naritan, K.; Niinomi, M.; Nakai, M. Effects of micro- and nano-scale wave-like structures on fatigue strength of a beta-type titanium alloy developed as a biomaterial. *J. Mech. Behav. Biomed. Mater.* **2014**, *29*, 393–402. [[CrossRef](#)] [[PubMed](#)]
13. Morais, L.S.; Serra, G.G.; Palermo, E.F.A.; Andrade, L.R.; Müller, C.A.; Meyers, M.A.; Elias, C.N. Systemic levels of metallic ions released from orthodontic mini-implants. *Am. J. Orthod. Dentofac. Orthop.* **2009**, *135*, 522–529. [[CrossRef](#)] [[PubMed](#)]
14. Djouina, M.; Esquerre, N.; Desreumaux, P.; Vignal, C.; Body-Malapel, M. Toxicological consequences of experimental exposure to aluminum in human intestinal epithelial cells. *Food Chem. Toxicol.* **2016**, *91*, 108–116. [[CrossRef](#)] [[PubMed](#)]
15. Zaffea, D.; Bertoldi, C.; Consolo, U. Accumulation of aluminium in lamellar bone after implantation of titanium plates, Ti-6Al-4V screws, hydroxyapatite granules. *Biomaterials* **2004**, *25*, 3837–3844. [[CrossRef](#)] [[PubMed](#)]
16. Czajka, M.; Sawicki, K.; Sikorska, K.; Popek, S.; Kruszewski, M.; Kapka-Skrzypczak, L. Toxicity of titanium dioxide nanoparticles in central nervous system. *Toxicol. In Vitro* **2015**, *9*, 1042–1052. [[CrossRef](#)] [[PubMed](#)]
17. Xue, W.; Liu, X.; Zheng, X.; Ding, C. In vivo evaluation of plasma-sprayed wollastonite coating. *Biomaterials* **2005**, *26*, 3455–3460. [[CrossRef](#)] [[PubMed](#)]
18. Sadjadi, M.S.; Ebrahimi, H.R.; Meskinfam, M.; Zare, K. Silica enhanced formation of hydroxyapatite nanocrystals in simulated body fluid (SBF) at 37 °C. *Mater. Chem. Phys.* **2011**, *130*, 67–71. [[CrossRef](#)]
19. Qian, S.; Liu, X. Cytocompatibility of Si-incorporated TiO₂ nanopores films. *Colloids Surf. B Biointerfaces* **2015**, *133*, 214–220. [[CrossRef](#)] [[PubMed](#)]
20. Hu, H.; Qiao, Y.; Liu, F.H.X.; Ding, C. Enhanced apatite-forming ability and cytocompatibility of porous and nanostructured TiO₂/CaSiO₃ coating on titanium, *Colloids Surf. B Biointerfaces* **2013**, *101*, 83–90. [[CrossRef](#)] [[PubMed](#)]
21. Li, G.; Cao, H.; Zhang, W.; Ding, X.; Yang, G.; Qiao, X.; Liu, X.; Jiang, X. Enhanced osseointegration of hierarchical micro/nanotopographic titanium fabricated by microarc oxidation and electrochemical treatment. *ACS Appl. Mater. Interfaces* **2016**, *8*, 3840–3852. [[CrossRef](#)] [[PubMed](#)]
22. Zulfdesmi, M.; Waki, A.; Kuroda, K.; Okido, M. Hydrothermal treatment of titanium alloys for the enhancement of osteoconductivity. *Mater. Sci. Eng. C* **2015**, *49*, 430–435. [[CrossRef](#)] [[PubMed](#)]
23. Han, G.; Müller, W.E.G.; Wang, X.; Lilja, L.; Shen, Z. Porous titania surfaces on titanium with hierarchical macro- and mesoporosities for enhancing cell adhesion, proliferation and mineralization. *Mater. Sci. Eng. C* **2015**, *47*, 376–383. [[CrossRef](#)] [[PubMed](#)]
24. Ueno, T.; Tsukimura, N.; Yamada, M.; Ogawa, T. Enhanced bone-integration capability of alkali- and heat-treated nanopolymorphic titanium in micro-to-nanoscale hierarchy. *Biomaterials* **2011**, *32*, 7297–7308. [[CrossRef](#)] [[PubMed](#)]
25. Zhang, W.; Wang, G.; Liu, Y.; Zhao, X.; Zou, D.; Zhu, C.; Jin, Y.; Huang, Q.; Sun, J.; Liu, X.; et al. The synergistic effect of hierarchical micro/nano-topography and bioactive ions for enhanced osseointegration. *Biomaterials* **2013**, *34*, 3184–3195. [[CrossRef](#)] [[PubMed](#)]
26. Kazek-Kęsik, A.; Leśniak, K.; Zhidkov, I.S.; Korotin, D.M.; Kukhareno, A.I.; Cholakh, S.O.; Kalembe-Rec, I.; Suchanek, K.; Kurmaev, E.Z.; Simka, W. Influence of alkali treatment on anodized titanium alloys in wollastonite suspension. *Metals* **2017**, *7*, 322. [[CrossRef](#)]
27. Kokubo, T. Apatite formation on surfaces of ceramics, metals and polymers in body environment. *Acta Mater.* **1998**, *46*, 2519–2527. [[CrossRef](#)]
28. Kazek-Kęsik, A.; Krok-Borkowicz, M.; Dercz, G.; Donesz-Sikorska, A.; Pamuła, E.; Simka, W. Multilayer coatings formed on titanium alloy surfaces by plasma electrolytic oxidation-electrophoretic deposition methods. *Electrochim. Acta* **2016**, *204*, 294–306. [[CrossRef](#)]

29. Wei, D.; Zhou, Y.; Jia, D.; Wang, Y. Chemical treatment of TiO₂-based coatings formed by plasma electrolytic oxidation in electrolyte containing nano-HA, calcium salts and phosphates for biomedical applications. *Appl. Surf. Sci.* **2008**, *254*, 1775–1782. [[CrossRef](#)]
30. Yang, Z.; Xia, L.; Li, W.; Han, J. Effect of Ca/P ratio on bioactivity of PEO coatings. *Adv. Biomed. Eng. Technol.* **2015**, *2*, 13–19. [[CrossRef](#)]
31. Yan, Y.; Han, H.; Lu, C.G. The effect of chemical treatment on apatite-forming ability of the macroporous zirconia films formed by micro-arc oxidation. *Appl. Surf. Sci.* **2008**, *254*, 833–839. [[CrossRef](#)]
32. Pan, Y.K.; Chen, C.Z.; Wang, D.G.; Lin, Z.G. Preparation and bioactivity of micro-arc oxidized calcium phosphate coatings. *Mater. Chem. Phys.* **2013**, *141*, 842–849. [[CrossRef](#)]
33. Robin, M.; Almeida, C.; Azaïs, T.; Haye, B.; Illoul, C.; Lesieur, J.; Giraud-Guille, M.N.; Nassif, N.; Hélyary, C. Involvement of 3D osteoblast migration and bone apatite during in vitro early osteocytogenesis. *Bone* **2016**, *88*, 146–156. [[CrossRef](#)] [[PubMed](#)]
34. Addison, W.N.; Nelea, V.; Chicatun, F.; Chien, Y.C.; Tran-Khanh, N.; Buschmann, M.D.; Nazhat, S.N.; Kaartinen, M.T.; Vali, H.; Tecklenburg, M.M.; et al. Extracellular matrix mineralization in murine MC3T3-E1 osteoblast cultures: An ultrastructural, compositional and comparative analysis with mouse bone. *Bone* **2015**, *71*, 244–256. [[CrossRef](#)] [[PubMed](#)]
35. Müller, W.E.G.; Tolba, E.; Schröder, H.C.; Muñoz-Espí, R.; Diehl-Seifert, B.; Wang, X. Amorphous polyphosphate-hydroxyapatite: A morphogenetically active substrate for bone-related SaOS-2 cells in vitro. *Acta Biomater.* **2016**, *31*, 358–367. [[CrossRef](#)] [[PubMed](#)]
36. Olszta, M.J.; Cheng, X.; Jee, S.S.; Kumar, R.; Kim, Y.Y.; Kaufman, M.J.; Douglas, E.P.; Gower, L.B. Bone structure and formation: A new perspective. *Mater. Sci. Eng. R* **2007**, *58*, 77–116. [[CrossRef](#)]



© 2018 by the authors. Licensee MDPI, Basel, Switzerland. This article is an open access article distributed under the terms and conditions of the Creative Commons Attribution (CC BY) license (<http://creativecommons.org/licenses/by/4.0/>).